AIAA JOURNAL
Vol. 43, No. 11, November 2005

Structure of Supersonic Twin Jets

M. B. Alkislar,* A. Krothapalli,† I. Choutapalli,‡ and L. Lourenco§
Florida A&M University and Florida State University, Tallahassee, Florida 32310

The flow characteristics of coupled oscillatory motion of $M_j = 1.5$ supersonic twin jets are described using the particle image velocimetry measurements. As a result of self-excitation caused by screech, sinuous oscillation of individual jets is observed. The coupling between the jets, characterized by the presence of coherent large-scale eddies, results in a symmetric mode with respect to the midplane separating the two jets. A control technique using microjets placed at the nozzle exit is used to suppress the unsteady flow. The results show that the predominant unsteady character of the twin jets is reduced considerably as a result of the elimination of large-scale organized structures with the introduction of the control. The turbulence levels show a 50% decrease in turbulent kinetic energy in the mixing region of the twinjet. Consequently, up to 4-dB reductions in overall sound pressure level of jet noise are observed. The reduction in noise and turbulence is accompanied by a decrease of about 20% in the entrainment of the ambient fluid around the jet.

I. Introduction

THE experiment described in this paper is a part of our ongoing effort to delineate the main flow and noise characteristics of supersonic jets using particle image velocimetry (PIV) and other standard measurement techniques. The problem addressed here is motivated by the use of twin jets in short-take-off-and-vertical-landing (STOVL) aircraft configurations similar to that of the Joint Strike Fighter. In the course of studying the twin-jet flows in ground effect, strong evidence of the unsteady flow behavior dominated by a strong-coupled motion was observed.[1] It appeared that the strong coupling of the individual freejet instability resulted in the oscillatory behavior and the jet impingement further strengthened it. With the unsteady flow being the source of noise generation, it is of practical interest to devise a technique to mitigate the coupled jet behavior. A novel control technique using microjet injection at the nozzle exit that was proven to be quite effective in large-scale eddy suppression in single supersonic impinging jet[2] is also employed in this study.

Seiner et al.[3] conducted experiments on two closely spaced supersonic freejets, operating at off-design conditions. Such jets are known to produce intense screech tones, and the dynamic loads associated with them can reach levels that could result in damage to structures placed at the nozzle exit. Tam and Seiner[4] found that the screech tone frequency of the twin jets was slightly different to that of a single jet and the acoustic intensity in the internozzle region exceeded that of the direct sum of two noninteracting screeching jets. A similar investigation using twin rectangular supersonic jet was carried out by Raman and Taghavi[5] to explore the role of nozzle spacing on the determination of different oscillatory modes (symmetric and antisymmetric) of the jets. The close coupling of multiple rectangular freejets is examined by Krothapalli et al.[6] using an edge tone generation in one of the jets. This experiment clearly showed that a discrete sound generated by one jet can interact with neighboring jets to create a coupled oscillatory flow resulting in large-eddy generation, thus producing enhanced mixing of multiple jets.

The main parameters that govern the twin-jet flowfield are the jet-exit Mach number, the nature of the jet expansion at the nozzle exit (ideally expanded, underexpanded or overexpanded), and the spacing between the jets and the jet-exit Reynolds number. In the present experiment, the jets are operated at ideally expanded condition at a jet-exit Mach number of 1.5. The spacing (distance between the centers of the individual nozzles) between the two jets is fixed at $3d$. (d is the exit diameter of the nozzle.) The Reynolds number based on the jet-exit velocity and nozzle-exit diameter is about 5.5×10^5.

In this, after describing the experimental setup, we show, using flow visualization and PIV data, the nature of the twin-jet coupling and its mitigation using microjet injection. Also studied is the effect of the large-scale jet oscillations on the entrainment field, which is known to be source of the suction pressures on the lift plate.

II. Experimental Apparatus and Procedures

The experiments were conducted in the STOVL supersonic jet facility of the Fluid Mechanics Research Laboratory located at the Florida State University. The facility was designed to obtain the jet-induced forces on a STOVL aircraft model hovering in and out of ground effect. To simulate the hover effect, the distance between the ground plane and the jet nozzle exit was varied by moving the ground plane vertically relative to the nozzle exit through a remote-control hydraulic lift incorporated with the facility. For the experiments described here, the ground plane was kept at farthest distance with the height of about 1.5 m or about 60 diameters away from nozzle exit in order to simulate freejet conditions. Flowfield measurements were obtained incorporating a PIV setup to the facility as shown schematically in Fig. 1.

The measurements were carried out with nearly ideally expanded jets with weak shock waves at nozzle pressure ratio = 3.7 (nozzle stagnation pressure/ambient pressure). The two identical nozzles were mounted on a plenum chamber assembly as illustrated in Fig. 2. Each jet existed from a converging–diverging (C-D) axisymmetric nozzle with a throat diameter of 18 mm designed for an exit Mach number of 1.5. The operating condition was kept at its nominal value within a pressure variation of ± 2 kPa and a temperature variation of ± 5 K, resulting in an error of ± 5 m/s (about 1%) in velocity. The exit diameter d of the C-D nozzle was 19.5 mm. The divergent section was intentionally made of straight conic section with a 3-deg divergence angle to mimic the realistic nozzle geometry used in practice. The nominal exit Reynolds number, based on the exit velocity U_j and nozzle diameter d, was about 5.5×10^5. The state of the nozzle-exit boundary layer was expected to be laminar based on the exit profile measurements performed previously under

Presented as Paper 2004-0011 at the AIAA 42nd Aerospace Sciences Meeting, Reno, NV, 5–8 January 2004; received 27 April 2004; revision received 22 September 2004; accepted for publication 22 October 2004.

*Research Associate, Department of Mechanical Engineering; currently Engineer/Scientist, P.O. Box 3707, MC 67-ML, Acoustics and Fluid Mechanics, Boeing Commercial Airplanes, Seattle, WA 98124-2207; Mehmet.B.Alkislar@boeing.com. Member AIAA.

†Don Fuqua Eminent Scholar and Professor, Department of Mechanical Engineering, 2525 Pottsdamer Street; kroth@eng.fsu.edu. Associate Fellow AIAA.

‡Ph.D. Student, Department of Mechanical Engineering, 2525 Pottsdamer Street; cisaac@eng.fsu.edu. Student Member AIAA.

§Professor, Department of Mechanical Engineering, 2525 Pottsdamer Street; lourenco@eng.fsu.edu. Member AIAA.

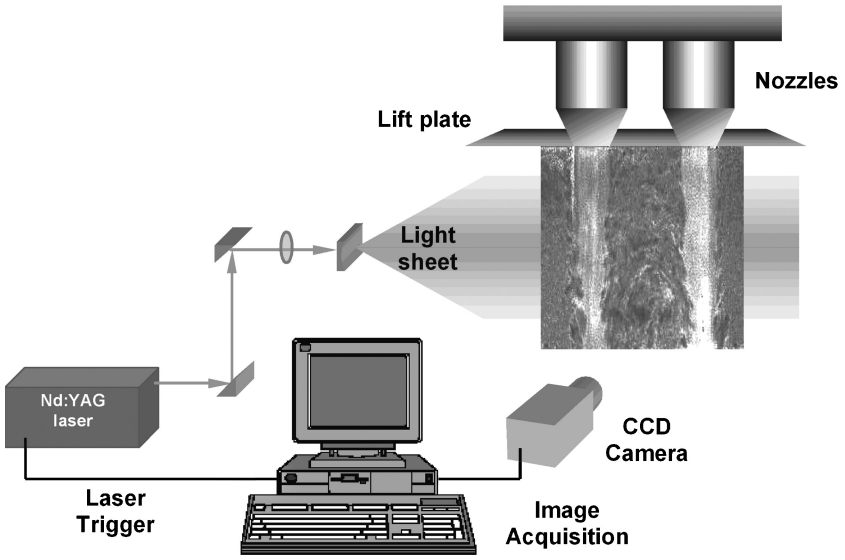

Fig. 1 Schematic arrangement of twin supersonic jet apparatus with the PIV setup.

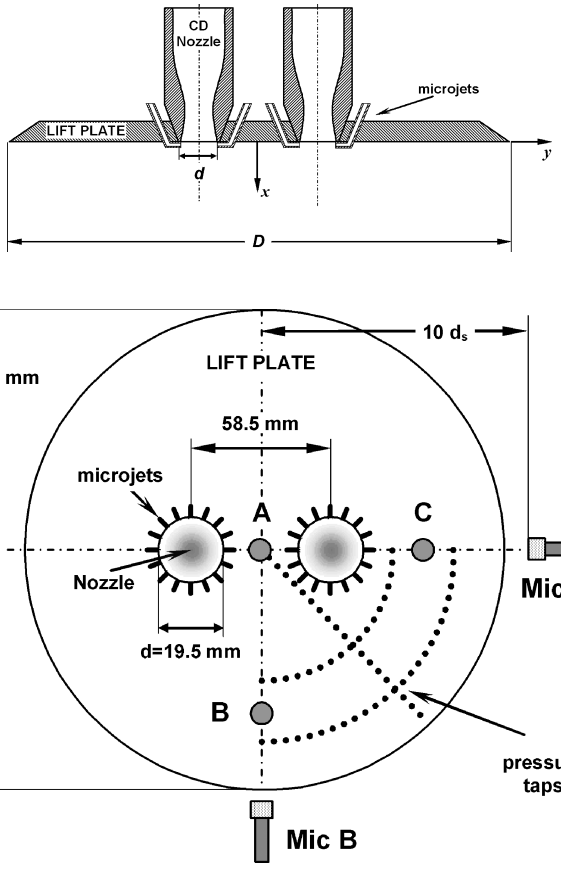

Fig. 2 Illustrations of nozzle and lift plate instrumentation: a) side view and b) bottom view. Kulite transducer locations are indicated by A, B, and C.

similar nozzle and operating conditions.[7] The distance between the nozzle centers was 58.5 mm ($\sim 3d$). The combined exit area of the two nozzles was identical to that of a single nozzle ($d_s = 27.5$ mm) used in Krothapalli et al.[8] An aluminum plate of 254-mm diam was flush mounted with the nozzles, which served as the lift plate for simulation of the aircraft surface from which the jets were issued. The coordinates x and y correspond to axial and radial directions of the jet, and u and v are respective velocity components. The origin of the coordinate system is centered on the lift plate as shown in Fig. 2a.

Sixteen microjets generated from a high-pressure source and exiting from 400-μm-diam tubes entered the primary jet at an angle of 90 deg to the nozzle axis (Fig. 2a). Nitrogen from a high-pressure gas cylinder was led to a cylindrical manifold through a pressure regulator, from which it was distributed to the 400-μm stainless-steel tubes to create the microjets. In the experiments, a combined mass flow rate of 0.0025 kg/s was used; this value corresponds to about 0.6% of the primary jet mass flux. The just-noted microjet mass flow rate was possible by maintaining effective stagnation conditions of $P_{0\text{mj}} = 100$ psig and $T_{0\text{mj}} = 300$ K. With these conditions, the microjet tube exit flow was choked, and the fully expanded Mach number was supersonic having a value of 1.5.

The lift plate contained 48 pressure taps arranged along radial and circumferential directions covering one-quarter of the lift plate (as indicated in Fig. 2b by dotted lines). The holes were spaced unevenly with closer spacing near the nozzle exit. The pressures were measured with a Validyne strain-gauge transducer mounted in a scanivalve unit. At each port, several seconds of digitized data were taken and processed later to obtain the mean surface pressure. The jet-induced mean surface pressures on the plate were used to calculate the lift force. The unsteady surface pressure was measured by three Kulite pressure transducers with 35-kPa range and ± 0.15-kPa accuracy located strategically on the lift plate. The signals were passed though a low-pass filter with a cutoff frequency of 33 kHz, before being digitized with a sampling rate of 70 kHz.

A quarter-inch Bruel&Kjaer microphone (Type 4136) with preamplifier (Type 2690A) was used for limited near-field acoustic measurements of jet noise. This microphone had a flat response up to 70 kHz and could be exposed to noise levels of about 170 dB. Two such microphones were used in the experiment. As shown in Fig. 2b, they were located in two different planes, 10 d_s away from the nozzle exit at an angle of 90 deg with respect to the jet inlet. The acoustic signals were passed through a low-pass filter with a cutoff frequency of 50 kHz and acquired with a sampling rate of 110 kHz. In the decibel range of the measurements, which was larger than the 120 dB, the maximum calculated error considering only microphone characteristics was within ± 1 dB. Several repetitions of the same experiment yielded a maximum of ± 1.5-dB variation in overall sound pressure level (OASPL).

For PIV measurements, a dual-cavity digitally sequenced Nd:YAG laser (Spectra Physics PIV400) was used. A light sheet of 1-mm thickness was created by suitable combination of spherical and cylindrical lenses (Fig. 1). The images were recorded by a cross-correlation Charge-Coupled-device camera (Kodak ES1.0) fitted with a 55-mm (f/1.4) Nikon lens. The resolution of the camera that was operated in double-exposure mode is 1k $\times$ 1k. In this mode of operation, with proper synchronization with laser pulses the camera could acquire at a rate of 15 image pairs per second. In

the experiments the jet was seeded with submicron (~0.3-μm) oil droplets generated by a modified Wright Nebulizer, which delivered the particles to the main jet. The flow rate of the seeding particles was controlled in such a way that there were enough particles in the jet. The ambient air was seeded with smoke particles (1–10 μm) produced by a Rosco fog generator. The measurements were confined to the central plane containing the two jets. A novel-processing algorithm developed by Lourenco and Krothapalli[9] was used to obtain accurate velocity data with high spatial resolution. Considering all diverse effects in the processing of PIV images of such flows, an error of 0.03 pixels was conservatively estimated in the particle displacement quantification. The time interval between the laser pulses was optimized to yield a maximum particle displacement of five pixels giving a relative error of 0.6%. Mean and turbulent velocity fields were computed by processing 1000 image pairs, thus giving an accuracy of better than 1 and 5% in mean velocity and turbulence intensity measurements respectively for the turbulence levels seen in the flowfield. For a more detailed discussion of the PIV setup and its accuracy, reference can be made to Alkislar et al.[10]

III. Results and Discussion

A. Flow Visualization

A conventional shadowgraph technique was used to visualize the twin-jet flow. The images were captured by using a super VHS (SVHS) video camera. Images displaying important flow features of the normal freejets are shown in Fig. 3 at two different time instants representative of two different phases of the resonance condition. An examination of the continuous video record suggests that the axisymmetric freejet instability manifests itself in symmetric as well as helical and/or flapping modes. But most often the two jets are dominated by the helical mode instability. The coupling between the jets results in a symmetric mode with respect to the midplane separating the two jets. A similar observation was made by Seiner et al.[3] and Tam and Seiner[4] for two underexpanded screeching jets that are spaced closer (1.9 d) than the current setup. The results of the stability analysis of Morris[11] clearly show for modes that are even about the symmetry plane between the two jets; the pressure levels in the internozzle region are much higher in the twin-jet case as compared to a single jet. Further, Green and Crighton[12] concluded that close-proximity interactions greatly destabilize the varicose mode of the coupled jet and greatly stabilize the sinuous mode. Raman and Taghavi[5] used the coupling of twin rectangular jets to examine the conditions for oscillatory mode selection—varicose vs sinuous. Their investigation suggests that the effective screech source location plays a role in mode selection.

The sinuous oscillation of individual jets is a result of self-excitation caused by screech. Owing to the straight divergent section, a weak shock cell structure is present in the jet. Together with the presence of lift plate, an intense screech tone is generated as shown in Fig. 4. The Strouhal number fd/U_e corresponding to the screech tone at 5816 Hz is 0.27 as compared to 0.31 for an equivalent single jet as reported by Krothapalli et al.[8] These observations are consistent with those of Seiner et al.[3] The broadband peak seen in the microphone spectrum at 10 kHz is representative of the broadband shock associated noise.

The activation of microjets at the nozzle exit not only eliminates the screech tones but also reduces the sound pressure level (SPL) over a wide range of frequencies as shown in Fig. 4. As will be discussed later, the interaction of the microjets with the primary jet shear layer generates streamwise vortices of significant strength,[13] which mitigate the large-eddy formation. The resulting

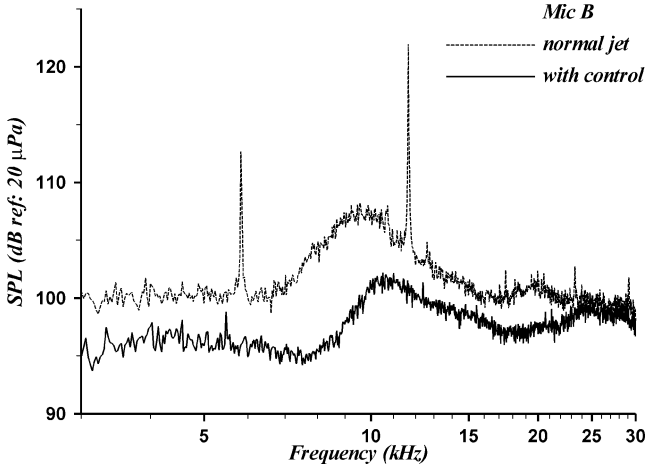

Fig. 4 Near-field microphone spectra for a twin freejet with and without control.

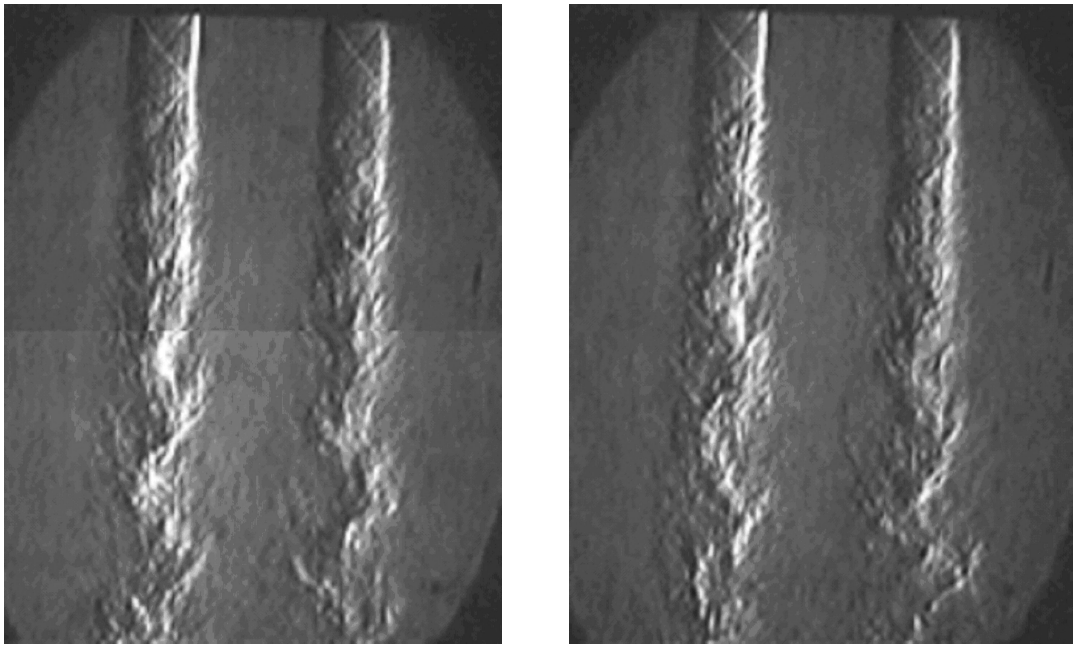

a) **b)**

Fig. 3 Shadowgraph pictures of twin freejets at $M = 1.5$.

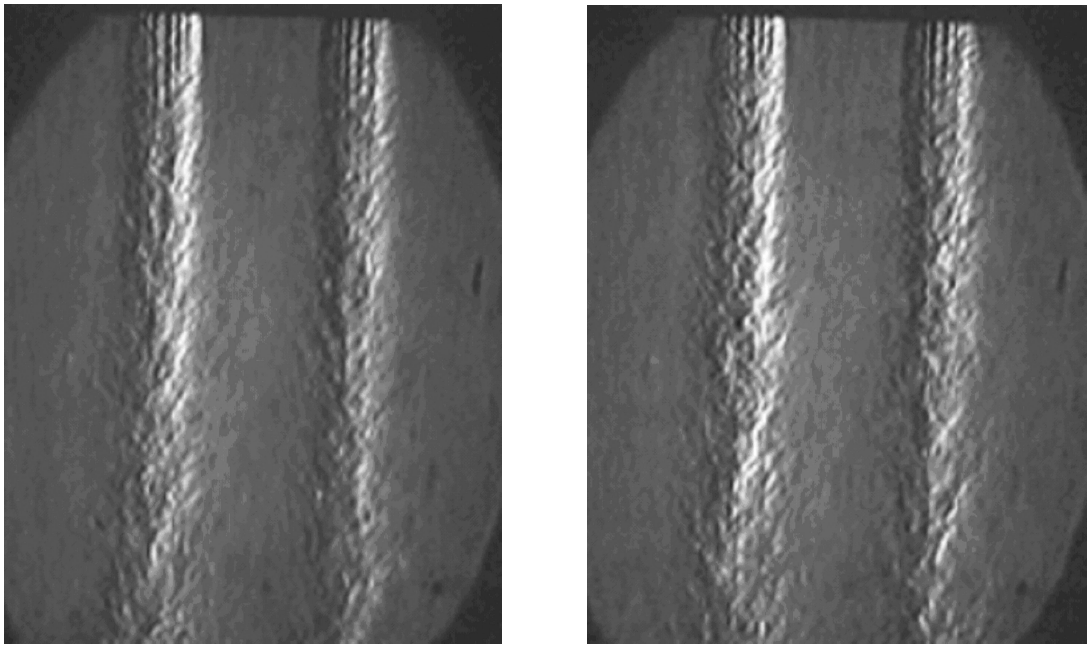

a) b)

Fig. 5 Shadowgraph pictures of the twin freejets with control at $M = 1.5$.

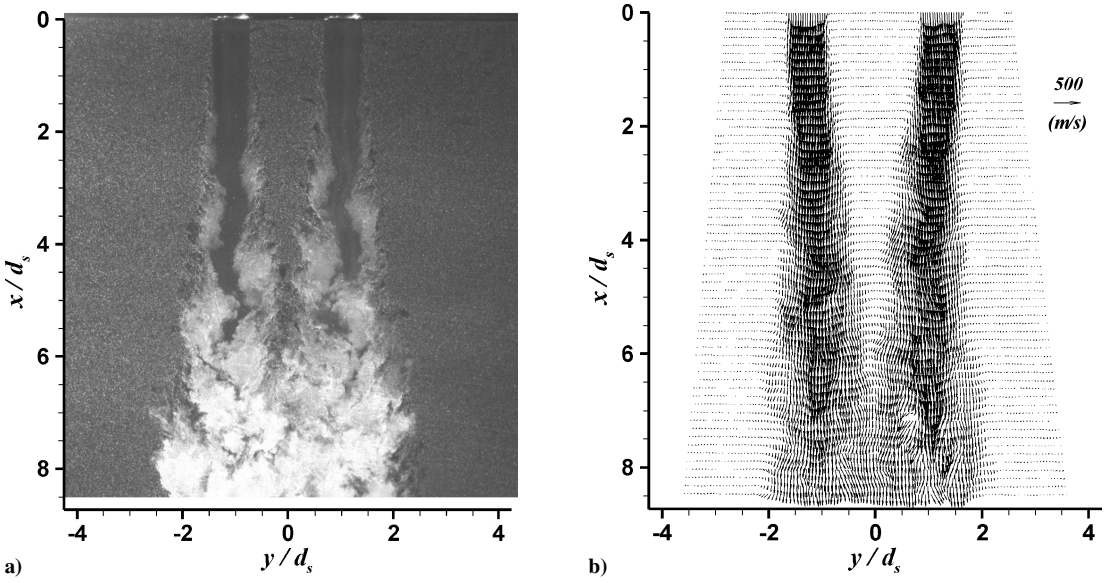

a) b)

Fig. 6 Ideally expanded normal jets at $M_j = 1.5$: a) instantaneous PIV image and b) the corresponding velocity vector field.

twin-jet flow shown in Fig. 5 clearly suggests that the large-eddy motion seen in Fig. 4 is absent. In addition, the pictures show vividly the footprints of the streamwise vortices at the nozzle exit. As many of jet noise suppression studies in our laboratory[14,15] indicate, the microjet injection is an effective control scheme to mitigate the formation of large-scale eddies, thereby creating a stable jet with reduced turbulence intensities. Hence, we will employ this technique here to suppress the unsteady behavior of the impinging jets.

B. PIV Flowfield Measurements

A detailed investigation of the twin-jet flowfield was carried out using the PIV technique. All of the measurements were confined to the central plane containing the two jets. The measurements of the jet flowfield and entrained flowfield were carried out in two different sets of experiments. A typical double-exposure image of the twin freejets and corresponding velocity field are shown in Fig. 6. The image clearly shows the coupled sinuous oscillation of the jets. The instantaneous velocity field was obtained using a 120×120 (x, y) trapezoidal grid. The uniformly scaled velocity vectors corresponding to the PIV image are also shown. The velocity data were obtained with great fidelity and very little data dropout. One thousand such velocity fields were obtained to yield statistical quantities that are necessary to describe the flowfield. The effect of control on the twin freejet instantaneous flowfield is seen in Fig. 7. The noninterfering nature of the jets, within the region of interest, is reflected with low velocities in between the jets. Because the entrainment flow is small in magnitude as compared with the jet velocity, it was measured separately, and a typical double-exposure image superimposed with the corresponding entrainment velocity field is shown in Fig. 8. For these measurements, the jet seeding was turned down significantly. The finite dimension of the lift plate with its sharp edge leads to

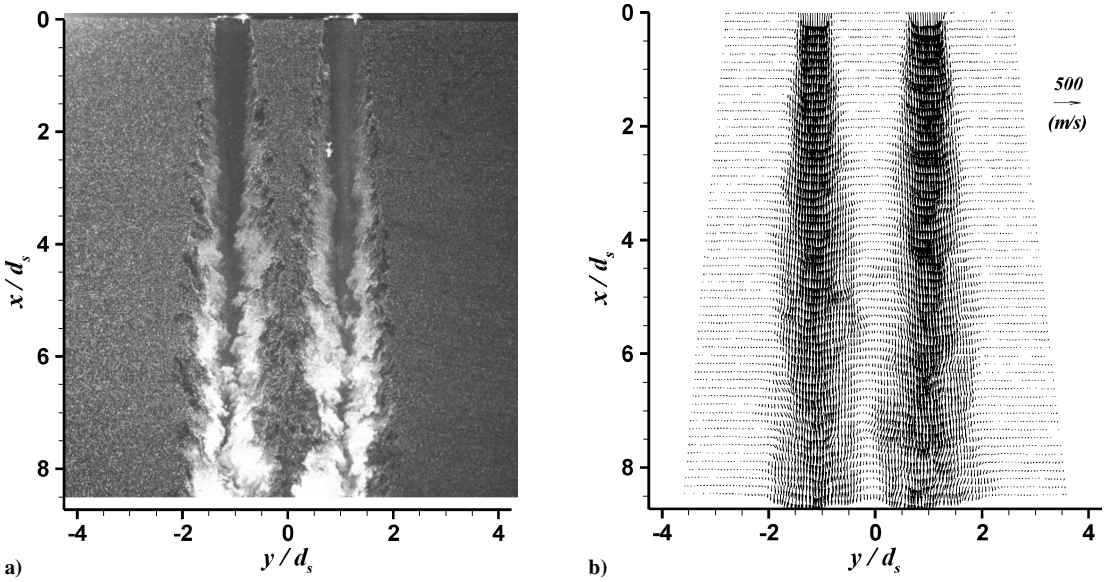

Fig. 7 Ideally expanded jets with control at $M_j = 1.5$: a) instantaneous PIV image and b) the corresponding velocity vector field.

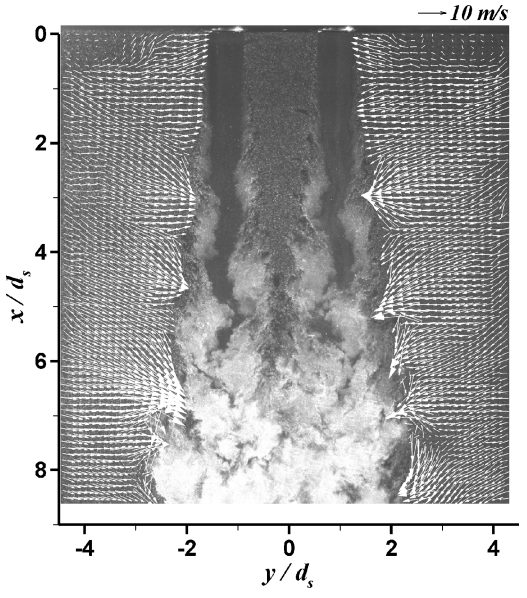

Fig. 8 Instantaneous PIV image superimposed with the corresponding entrainment velocity field.

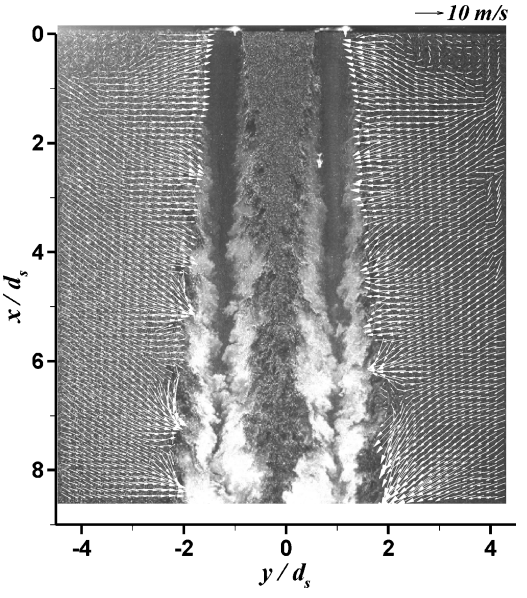

Fig. 9 Instantaneous PIV image superimposed with the corresponding entrainment velocity field for a controlled jet.

separation that is manifested in a recirculating bubble as shown in the top of the figure. The large-scale eddies generated as a result of sinuous coupled oscillations of the jet, for $x/d_s > 5$, are noticeable by their relatively large entrainment velocities in the near hydrodynamic field. For example, the typical velocity magnitude at the location of a large eddy is measured to be about 20 m/s as compared to about 6 m/s within the first few diameters of the nozzle exit. When the microjets at the nozzle exit are activated, the sinuous oscillations of the jets are alleviated as shown in Fig. 9. The corresponding entrainment velocity magnitudes are relatively small, typically about 5 m/s, an indication of diminished large-scale eddying motion.

1. Mean Jet Flowfield

The mean flow behavior was investigated using the average of 1000 instantaneous velocity fields. The mean velocity fields in the central XY plane for normal and controlled jets are shown in Figs. 10a and 10b, respectively. The axial mean velocity profiles at different downstream locations are superimposed on the normalized axial mean velocity represented by color contours. The symmetric nature of the mean velocity field, with respect to the midplane between the individual jets, is vividly displayed. The individual jets begin to merge at $x/d_s = 4.5$, a distance that is about 1.5 times the spacing between the jets. With the control, the shear layers downstream of merging show slower growth rate than those of the normal jets (Fig. 10a). Because of microjet injection at the nozzle exit, the shear layers within the first few diameters of the jet show a rapid growth (Fig. 10b).

The mean axial velocity variations along the centerline of one of the jets and in the symmetry plane of the two jets, corresponding to the flowfields shown in Fig. 10, are given in Fig. 11. The sinusoidal variation of the centerline velocity within the first few diameters is indicative of the presence of a weak shock structure in the jet. As mentioned earlier, such a shock cell structure can aid the self-sustained oscillation of the jet. At about $x/d_s = 4$, the potential core ends, and the axial velocity starts to decrease as a result of the mixing. The difference in the decay rate is noticeable between the normal jet and the jet with control. For $x/d_s < 4$, the microjet activation seems to have little influence both on the centerline velocity and the symmetry plane velocity. This information confirms that

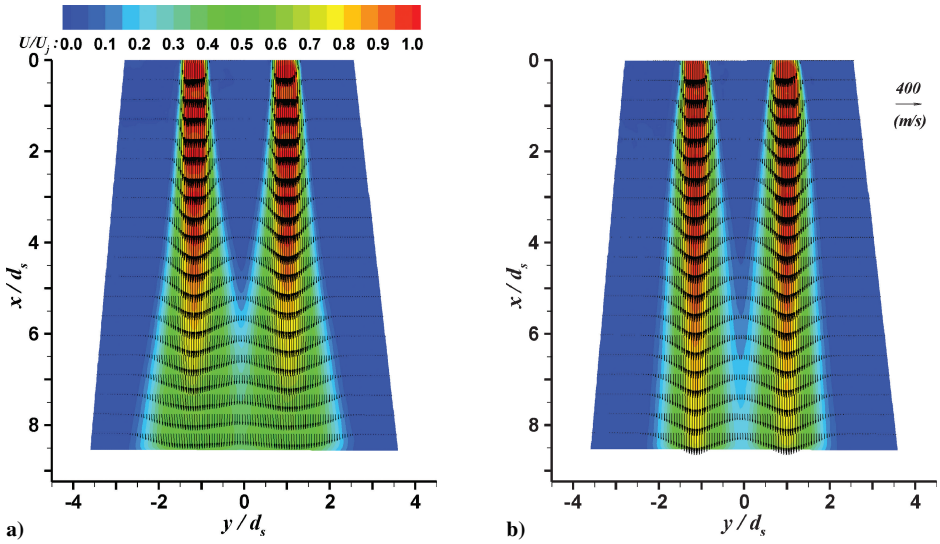

Fig. 10 Mean axial velocity field at $M_j = 1.5$: a) normal jet and b) with control.

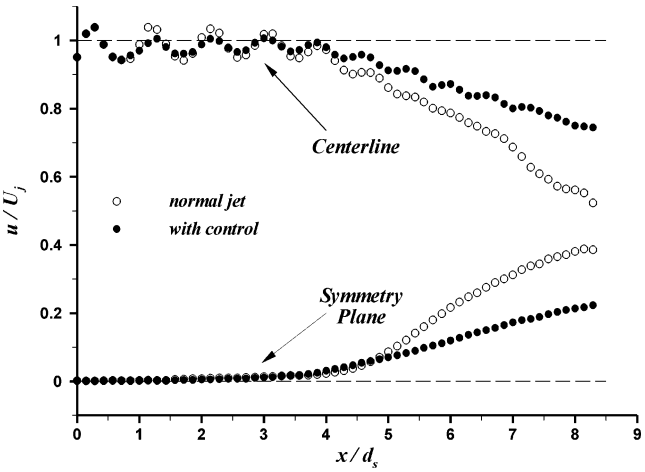

Fig. 11 Axial velocity profile comparisons at the jet centerline and midplane between the twin jets.

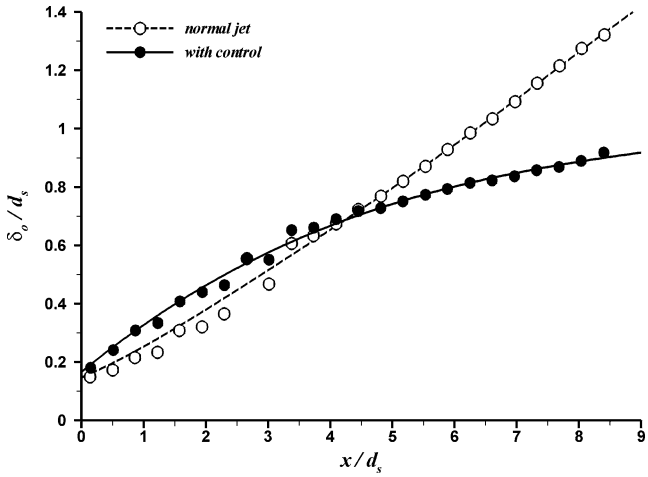

Fig. 12 Comparison of the outer shear-layer growth of normal jet and jet with control.

the suppression of the screech tones is caused by the elimination of large-scale structures in the shear layer by microjet control instead of any change in the shock cell structure. Farther downstream, the stabilization effect of the jets caused by control is quite evident with slower centerline velocity decay of the individual jet. Similarly, the axial velocity profile along the symmetry plane suggests the reduced growth rate of the shear layers.

To determine the effect of microjet control, the outer shear-layer growth was calculated using the mean velocity field data. The shear-layer thickness δ_o was defined as the distance between the locations where the axial velocity was equal to 5% ($u = 0.05U_c$) and 95% ($u = 0.95U_c$) of the local axial centerline velocity. The variations of the normalized shear-layer thickness for a jet with and without control are shown in Fig. 12. The shear-layer thickness of the jet with control shows a modest increase relatively to the normal jet for $x/d_s < 4$, whereas, for $x/d_s > 4$, a significant decrease is observed as plotted in the figure. The increased shear-layer thickness can be attributed to the enhanced mixing caused by streamwise vortices created by the interaction of the microjets with the jet flow. To show the generated streamwise vortical structures, recent data obtained from another study that was performed at another facility are given in Fig. 13. The out-of-plane component of the vorticity field, obtained using stereoscopic PIV, in the cross plane of a $M_j = 0.9$ jet at $x/d = 1.75$ is shown. In this experiment, eight microjets exiting from 800-μm-diam tubes entered the primary jet at an angle of 60 deg to the jet axis at the circular nozzle exit with a diameter of 70 mm. The presence of streamwise vorticity, which is contained in two counter-rotating vortices for each microjet, is vividly depicted in this figure with its normalized magnitude represented in color contours. Shear-layer boundary is also shown in the figure by the contour lines representing the axial velocity values of 0.1 U_j and 0.9 U_j. More recently, similar streamwise vortical structures are also seen in single $M_j = 1.5$ supersonic jet by Lou.[13] It was shown by Arakeri et al.[14] that the effect of microjets on the mean velocity parameters is limited to an axial distance of $x/d = 4$. However, the injection of streamwise vorticity into the shear layers reduces the growth of the shear layers much further downstream as shown in the Fig. 12. For a detailed description of the role of microjets on the development of an axisymmetric jet, reference can be made to Arakeri et al.[14] Although not shown in Fig. 12, similar growth behavior was observed for the inner shear layers between the jets.

2. *Mean Entrainment Flowfield*

The mean entrainment flowfields obtained from 1000 instantaneous vector fields are shown in Fig. 14. Previously shown main jet flow is superimposed onto the results to show the character of the jets. The recirculation bubble just mentioned is easily identified with blue regions near the lift plate. In the presence of microjets, relatively large magnitudes of entrainment velocities are measured at the nozzle exit as shown in Fig. 14b. This can be attributed to the

presence of strong streamwise vortical structures generated by the microjets.

The entrainment mass flow rate was calculated from the mean velocity field using control surfaces along the shear layer. The control surface was defined as a cylindrical area around one of the jets (left in figures) with a radius y_L, measured from the axis of the jet, with a length extending between the range $0.5 < x/d_s < 8.5$. The results are compared in Fig. 15. The figure shows that a reduction of about 20% in total entrainment mass flow rate occurs when the microjet control is enabled. With increasing y_L the mass flow rate increases because of increasing peripheral area, although entrainment velocities decrease in general. The increased entrainment in normal jet is caused by the large eddies present in the shear layers, which are known to decrease the static pressure on the lift plate.[8]

3. Turbulence Field

For brevity, the turbulence field is represented by the turbulence kinetic energy defined here by $(\overline{u'^2} + \overline{v'^2})$. The turbulence kinetic energy (TKE) normalized by the fully expanded jet velocity, represented by the color contours, is given in Fig. 16 for the jet conditions of Fig. 10. The magnitudes of the turbulence intensities for the controlled case are substantially reduced in the mixing region as compared to the normal jets, consistent with other observations of reduced unsteadiness in the controlled jets. The magnitude of fluctuations in the initial shear layer of controlled jets remains close to normal jet conditions with a subtle decrease.

A detailed examination of the changes in the flow brought about by the control is carried out using cross-plane mean and turbulence velocity profiles at selected locations of $x/d_s = 5$ and 8. The results are presented in Fig. 17. Shown in Fig. 17a, the subtle changes observed in the mean velocity profile at $x/d_s = 5$ are quite similar to those observed by Arakeri et al.[14] These authors have shown that the changes in profile, albeit quite small, can cause substantial changes in the turbulence characteristics of the shear layer as shown in Figs. 17b–17d. The changes in the mean velocity and the reductions in turbulence are more pronounced at downstream locations as indicated by the profiles shown in Figs. 17e–17h. Significant (~50%) reductions are measured in the transverse component rms velocity.

C. Unsteady Pressure Measurements

The narrowband frequency spectra of the Kulite's surface pressure signals on the lift plate (see Fig. 2b for sensor locations), corresponding to the conditions of Fig. 3, are shown in Fig. 18. The sinuous oscillation of individual jets is a result of self-excitation caused by screech. In the presence of lift plate and the weak shock cell structure, an intense screech tone is generated as shown in Fig. 4. The Strouhal number fd/U_j corresponding to the screech tone at 5.8 kHz is 0.27. The unsteady surface-pressure spectra given in Fig. 18 show a dominant tone at the screech frequency.

The microjet injection results in the mitigation of the dominant tone along with modest reductions at other frequencies as shown in Fig. 18a, quite similar to those seen in the near-field noise (Fig. 4). To

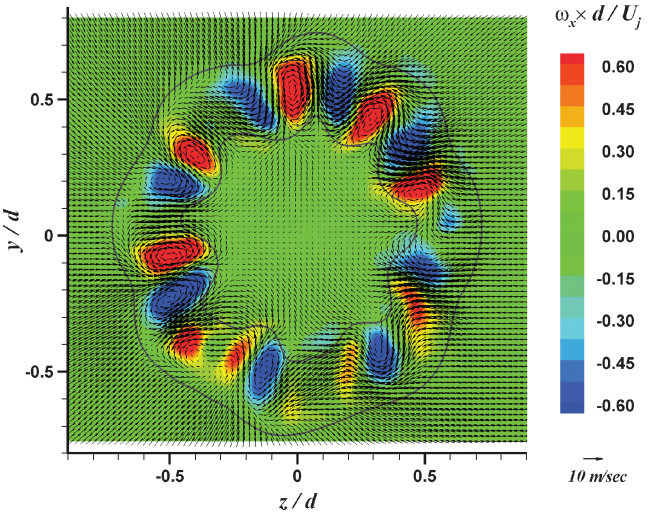

Fig. 13 Cross-plane streamwise vorticity distribution at $x/d = 1.75$, where $M_j = 0.9$.

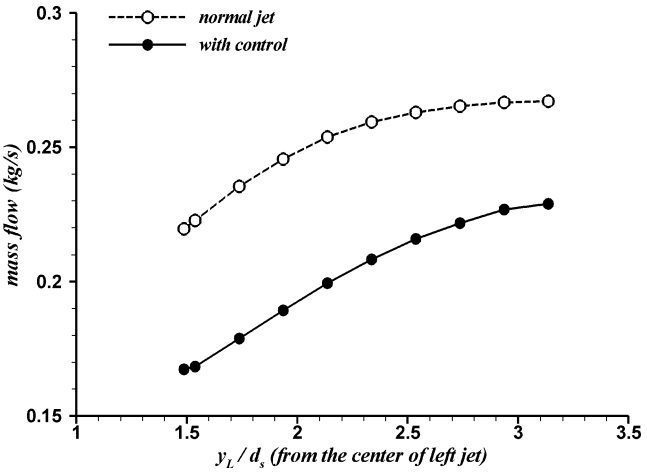

Fig. 15 Entrainment mass flow rate variation with downstream distance.

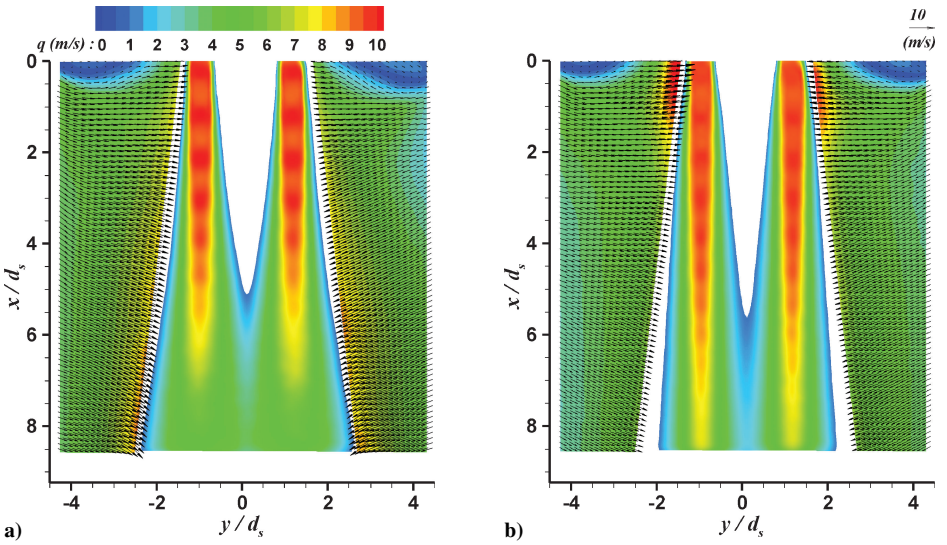

Fig. 14 Mean entrainment velocity field: a) normal jet and b) with control.

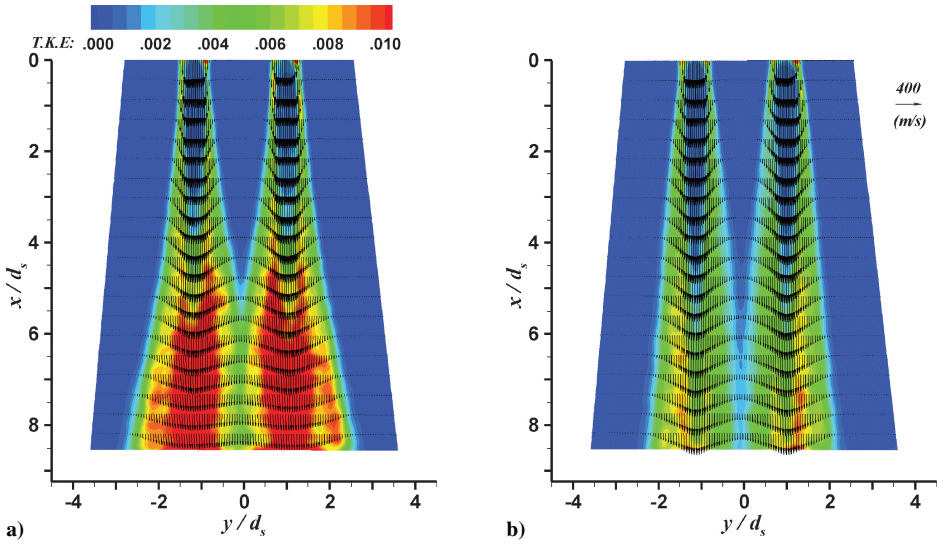

Fig. 16 Turbulent kinetic energy [$TKE = (\overline{u'^2} + \overline{v'^2})/U_j^2$] distribution for a) normal and b) controlled jet.

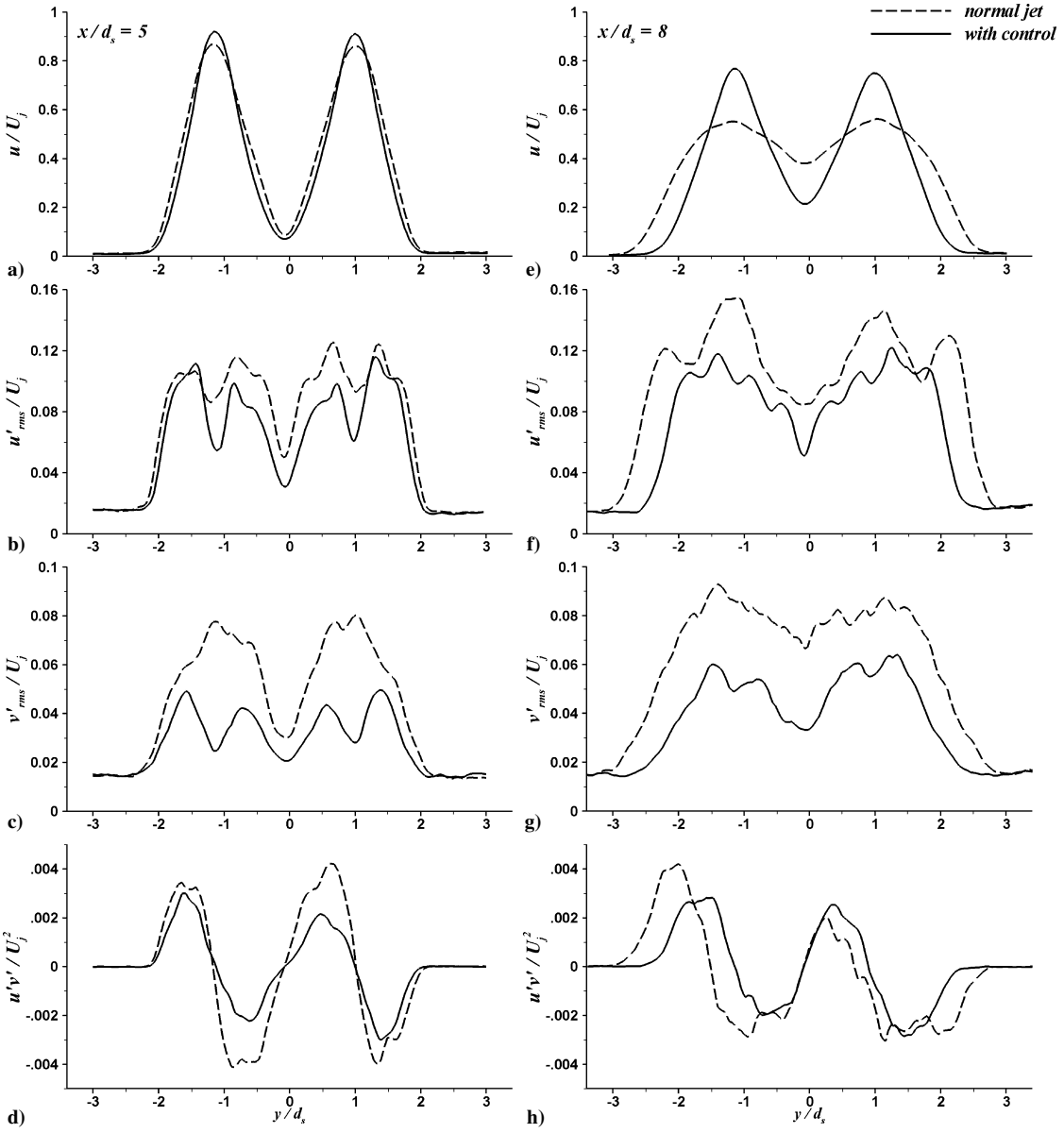

Fig. 17 Cross-plane normalized mean and turbulence velocity profiles at $x/d_s = 5$ and 8.

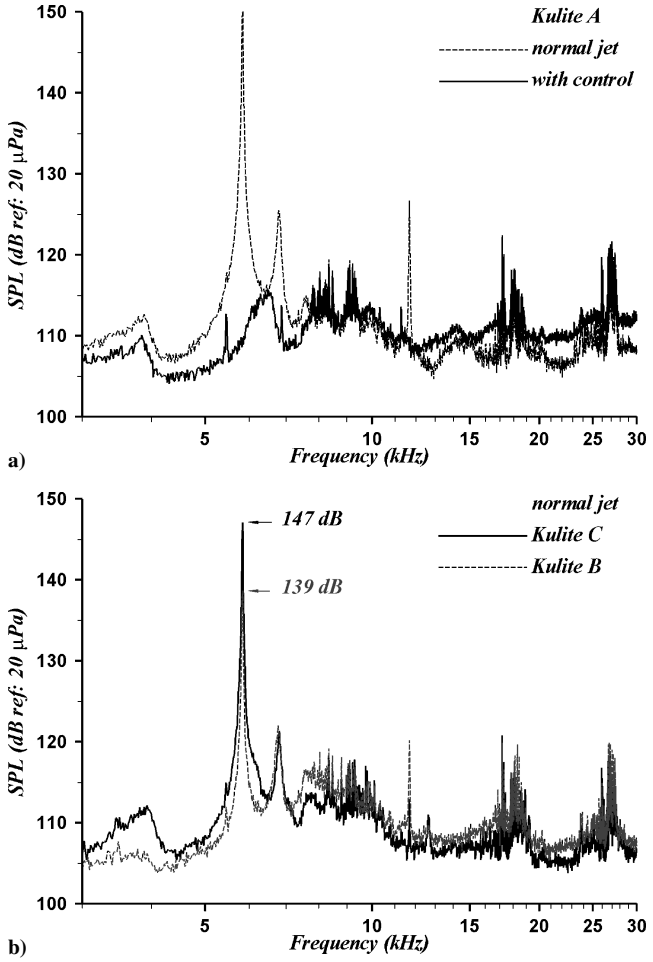

Fig. 18 Narrowband frequency spectra of the surface-pressure fluctuations: a) Kulite A location for normal jet and with control and b) normal jet for Kulite B and C locations (see Fig. 2).

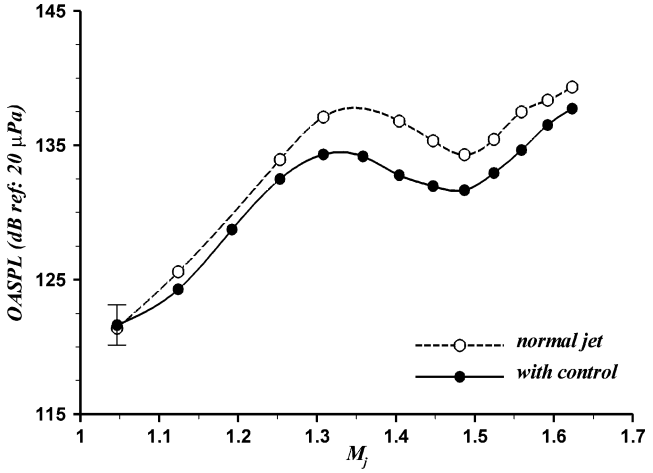

Fig. 19 Comparison of normal jet with controlled jet for measured OASPL variation with fully expanded jet Mach number.

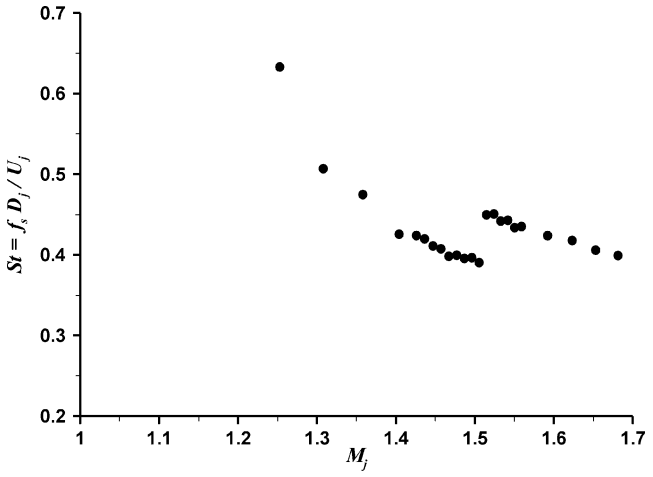

Fig. 20 Dominant tone Strouhal-number variation with fully expanded jet Mach number.

gain some understanding of the oscillatory mode behavior, the comparison of surface-pressure fluctuations is made in Fig. 18b between sensors Kulite B and C. The spectrum shows that the amplitude at discrete tone is 8 dB lower for Kulite B, which is located in the central plane between the jets, compared to Kulite C. This behavior shows that the dominant jet oscillations (flapping) occur in the plane containing the two jets. The comparison between Figs. 18a and 18b also shows that Kulite C has a spectrum very similar to that of Kulite A, although pressure levels are slightly lower because of shielding effect of the jet.

The OASPL calculated from the microphone A signal is shown in Fig. 19 with a varying fully expanded Mach number. First, the noise level increases with the increasing Mach number. Then, at about $M_j = 1.3$ it reaches to its local maximum in the overexpanded operating regime and then starts to decrease approaching to its local minimum at ideally expanded jet condition of $M_j = 1.5$. In the underexpanded operating regime, it resumes its increase with Mach number. Although not shown here, at an ideally operated jet condition the measurements with microphone B, which is along the midplane between the two jets, has 3.5 dB lower OASPL values than microphone A, which is positioned in the same plane as the jets (see Fig. 2b). A similar observation was made for the surface-pressure measurements as the Kulite C gave an OASPL value about 5 dB higher than Kulite B, confirming the previous observation that the dominant flapping mode is in the same plane with the jets.

When the microjet control is enabled, the OASPL decreases in all operating conditions as shown in Fig. 19. At certain operating conditions, as high as 4-dB reductions have been observed in the acoustic near field. At an ideally expanded jet condition, the microphone A and surface-pressure signals from Kulite A transducer show reductions of about 3 and 4 dB, respectively. The reductions are thought to be associated with the disruption of the generation of large coherent vortices in the feedback loop of screech phenomenon, leading to a marked reduction in the flow unsteadiness.

The variation of the Strouhal number (based on the fundamental tone frequency, fully expanded jet diameter and velocity) with the fully expanded Mach number is shown in Fig. 20. In the SPL spectra of acoustic signals no secondary tones, other than the fundamental screech tone and its harmonics, were observed. A jump in the Strouhal number at $M_j = 1.5$ is observed when the operating condition of the jet is changed from the overexpanded to underexpanded condition. Such a jump is generally attributed to a change in the oscillatory mode of the jet in screeching jets. In supersonic jets with sonic nozzles, several modes, as many as six,[3] have been reported. However, in the present study with a design Mach number of 1.5, only two modes can be identified from the acoustic data, and no visual distinction can be made between the two modes. Visually similar modes suggest that the staging can be a shift from a lateral mode (B) to a helical mode (C) as observed by Powell et al.[16] in single circular jet with sonic nozzle and by Umeda and Ishii[17] in twin jets.

IV. Conclusions

The effect of a simple control technique on the acoustic and aerodynamic characteristics of ideally expanded twin-jet flowfield was investigated. As a control method, a set of microjets was used around the jet exit. Microphone and dynamic surface-pressure measurements were used to observe the changes in the jet acoustics and sonic fatigue, and particle image velocimetry was used to measure

the aerodynamic characteristics of the jet in the presence of the control.

The microjet control appears to change the shear-layer characteristics, and it mitigates the violent unsteady behavior of the mixing regions. In addition, it prevents (or delays considerably) the formation of large-scale structures seen in coupled jets. Consequently, the turbulence levels in the mixing region of the jet decrease about 50%. Accordingly, a large reduction in the entrained flow is observed. Additional measurements of the entrainment flowfield show a 20% decrease in entrained mass flow. With control, near-field microphone measurements show an overall-sound-pressure-level reduction of about 4 dB. Concomitantly, the unsteady surface-pressure measurements on the lift plate show a reduction of about 5 dB.

Acknowledgments

We thank NASA Ames Research Center for supporting the work. We thank Jim Ross and Doug Wardwell for their continued interest in this problem.

References

[1]Elavarasan, R., Venkatakrishnan, L., Krothapalli, A., and Lourenco, L., "Supersonic Twin Impinging Jets," AIAA Paper 2000-0812, Jan. 2000.

[2]Alvi, F. S., Elavarasan, R., Shih, C., Garg, G., and Krothapalli, A., "Control of Supersonic Impinging Jet Flows Using Microjets," *AIAA Journal*, Vol. 41, No. 7, 2003, pp. 1347–1355.

[3]Seiner, J. M., Manning, J. C., and Ponton, M. K., "Dynamic Pressure Loads Associated with Twin Supersonic Plume Resonance," *AIAA Journal*, Vol. 26, No. 8, 1988, pp. 954–960.

[4]Tam, C. K. W., and Seiner, J. M., "Analysis of Twin Supersonic Plume Resonance," AIAA Paper 87-2695, Oct. 1987.

[5]Raman, G., and Taghavi, R., "Coupling of Twin Rectangular Supersonic Jets," *Journal of Fluid Mechanics*, Vol. 354, 1998, pp. 123–146.

[6]Krothapalli, A., Karamcheti, K., Hsia, Y., and Baganoff, D., "Edge Tones in High-Speed Flows and Their Application to Multiple-Jet Mixing," *AIAA Journal*, Vol. 21, No. 7, 1983, pp. 937, 938.

[7]Wishart, D. P., "The Structure of a Supersonic Heated Jet Operating at Design and Off-Design Conditions," Ph.D. Dissertation, Dept. of Mechanical Engineering, Florida State Univ., Tallahassee, FL, 1995.

[8]Krothapalli, A., Rajakuperan, E., Alvi, F., and Lourenco, L., "Flow Field and Noise Characteristics of a Supersonic Impinging Jet," *Journal of Fluid Mechanics*, Vol. 392, 1999, pp. 155–181.

[9]Lourenco, L., and Krothapalli, A., "True Resolution PIV: A Mesh-Free Second-Order Accurate Algorithm," *Proceedings of the 10th International Symposium on Applications of Laser Techniques in Fluid Mechanics*, Lisbon, 2000.

[10]Alkislar, M. B., Krothapalli, A., and Lourenco, L. M., "Structure of a Screeching Rectangular Jet: a Stereoscopic PIV Study," *Journal of Fluid Mechanics*, Vol. 489, 2003, pp. 121–154.

[11]Morris, P. J., "Instability Waves in Twin Supersonic Jets," *Journal of Fluid Mechanics*, Vol. 220, 1990, pp. 293–307.

[12]Green, M. R., and Crighton, D. G., "Instability Properties of Interacting Jets," *Journal of Fluid Mechanics*, Vol. 350, 1997, pp. 331–349.

[13]Lou, H., "Control of Supersonic Impinging Jets Using Microjets," Ph.D. Dissertation, Dept. of Mechanical Engineering, Florida State Univ., Tallahassee, FL, 2005.

[14]Arakeri, V. H., Krothapalli, A., Siddavaram, V., Alkislar, M. B., and Lourenco, L., "On the Use of Microjets to Suppress Turbulence in a Mach 0.9 Axisymmetric Jet," *Journal of Fluid Mechanics*, Vol. 490, 2003, pp. 75–98.

[15]Krothapalli, A., Greska, B., and Arakeri, V., "High-Speed Jet Noise Reduction Using Microjets," AIAA Paper 2002-2450, May 2002.

[16]Powell, A., Umeda, Y., and Ishii, R., "Observations of the Oscillation Modes of Chocked Circular Jets," *Journal of the Acoustical Society of America*, Vol. 92, No. 5, 1992, pp. 2823–2836.

[17]Umeda, Y., and Ishii, R., "Oscillation of Supersonic Multijets Exhausting from Very Adjacent Multiple Nozzles," *Journal of the Acoustical Society of America*, Vol. 110, No. 4, 2001, pp. 1873–1877.

R. Lucht
Associate Editor